Conformational Studies of Globular Proteomimetic Brush Polymers of Structured and Unstructured Peptides

Julia Oktawiec,[a] Omar M. Ebrahim,[a] Yu Chen,[b] Kaylen Su,[c] Christopher Sharpe,[b] Nathan D. Rosenmann,[b] Clara Barbut,[a] Steven J. Weigand,[d] Matthew Thompson,[a] James Byrnes,[e] Baofu Qiao,[c] Nathan C. Gianneschi[a,b,f]

[a] Department of Chemistry, Northwestern University, Evanston, IL 60208

[b] Department of Materials Science and Engineering, Northwestern University, Evanston, IL 60208

[c] Department of Natural Sciences, Baruch College, City University of New York, New York, NY 10010

[d] DuPont−Northwestern−Dow Collaborative Access Team (DND-CAT) Synchrotron Research Center, Northwestern University, Argonne, IL 60208

[e] Beamline 16ID, NSLS-II, Brookhaven National Laboratory, Upton, NY, 11973

[f] International Institute for Nanotechnology, Chemistry of Life Processes Institute, Simpson Querrey Institute, Lurie Cancer Center, Department of Biomedical Engineering, and Department of Pharmacology, Northwestern University, Evanston, IL 60208.

KEYWORDS. Peptide brush polymer; peptide folding; peptide materials, conformational characterization

ABSTRACT: Peptide-brush polymers generated by graft-through living polymerization of peptide-modified monomers exhibit high proteolytic stability, therapeutic efficacy, and potential as functional tandem repeat protein mimetics. Prior work has focused on polymers generated from structurally disordered peptides that lack defined conformations. To obtain insight into how the structure of these polymers is influenced by the folding of their peptide sidechains, a set of polymers with varying degrees of polymerization was prepared from peptide monomers that adopt α-helical secondary structure for comparison to those having random coil structures. Circular dichroism and nuclear magnetic resonance spectroscopy confirm the maintenance of the secondary structure of the constituent peptide when polymerized. Small-angle X-ray scattering (SAXS) studies reveal the solution-phase conformation of PLPs in different solvent environments. In particular, X-ray scattering shows that modulation of solvent hydrophobicity, as well as hydrogen bonding patterns of the peptide sidechain, plays an important role in the degree of globularity and conformation of the overall polymer, with polymers of helical peptide brushes showing less spherical compaction in conditions where greater helicity is observed. These structural insights into peptide brush folding and polymer conformation inform the design of these proteomimetic materials with promise for controlling and predicting their artificial fold and morphology.

The ability to discover and develop peptides to specifically target and bind proteins has resulted in an increasing interest in peptide-based or peptidomimetic therapeutics.[1–4] However, cellular penetration, resistance to proteolysis[5] and multivalent, high avidity binding to intracellular targets remain challenges facing the translational potential of peptides generally. To this end, cyclization,[6–8] lipidation,[9–11] and peptide-stapling approaches[12–14] have been and remain key strategies for enabling the development of peptides and peptidomimetics.[15,16] An emerging strategy involves coupling a polymerizable moiety to a peptide of interest to yield a peptidyl-macromonomer that is then subjected to graft-through polymerization using ring-opening metathesis polymerization (ROMP)[17,18] or controlled radical polymerization chemistry, including photoinduced reversible addition−fragmentation transfer radical polymerization (RAFT).[19,20] The resulting peptide-brush polymers show enhanced resistance to proteolysis,[18] as well as the ability to internalize into cells and to access intracellular, cytosolic targets with high affinities.[21–24] The observed elevated resistance to proteolysis is ascribed to the collapsed globular structures of the polymers observed in water that arise, in particular in the case of brush polymers generated from norbornenyl-peptides (polynorbornenes), due to backbone hydrophobicity driving an entropically favorable collapse. This collapse leads to sterically crowded peptide brushes, rendering them less accessible to proteases, while preserving their ability to interact with therapeutic targets and cellular membranes due to polymer dynamics.[18,20] As a result of these collective, emergent properties, we refer to these materials as Protein-Like Polymers (PLPs).[22,25]

Despite initial success in implementing this strategy to achieve desired biological properties and outcomes, an in-depth understanding of how the polymer backbone influences the folding and conformation of such peptide brushes, and vice versa, is needed. One related example involves brush polymers of poly(γ-benzyl-L-glutamate) generated using norbornene monomers with variable lengths of poly(γ-benzyl-L-glutamate) segments.[26] The helicity of these polymers was assessed using

^{1}H NMR spectroscopy in 2% TFA-d/$CDCl_3$, and it was found that brush polymers had slightly lower degrees of helicity than the poly(γ-benzyl-L-glutamate) segments by themselves. The interruption of folding was reduced when grafting density was lessened. Similar polymers generated by post-polymerization modifications have been shown to form rod-like structures by dry-state atomic force microscopy.[27] In general, experimental and computational studies find that while hydrophobic environments can promote helicity of peptide amphiphiles,[28,29] steric crowding can also interrupt the uniform folding of peptides into helices.[30]

Our motivation to understand these effects lies in the ability to control folding and structure in a cooperative way, which will influence the utility of these materials in a range of settings. Greater structural insight into more complex peptide-brush polymers would allow for the determination of structure-function relationships for the targeted design of peptide-brush polymer tools for engaging specific protein targets. In particular, it may be important to preserve the organization of functional groups on the face of helical peptide side chains, so that they can readily inhibit particular protein–protein interactions involved in disease progression.[31,32] Herein, a particular focus was to establish whether helicity could be preserved or enhanced in aqueous environments when an α-helical peptide is incorporated onto a polymer backbone. Approaches described here were inspired, in part, by efforts to characterize the folding of single-chain nanoparticle polymers using techniques including small-angle X-ray scattering (SAXS).[33–39]

Towards this end, polymers were designed to contain brushes of peptides with a classical secondary structure, the α-helix, as well as a peptide with an unstructured, random coil configuration (**Fig. 1**). Using these peptides as macromonomers allows the use of techniques probing the perturbation of peptide folding, such as circular dichroism (CD) spectroscopy and nuclear magnetic resonance (NMR) spectroscopy. A set of polymers incorporating these peptide monomers was generated and studied using spectroscopy and X-ray scattering, coupled with atomistic metadynamics simulations, to gain a granular understanding of peptide folding and polymer conformation.

DISCUSSION

POLYMER DESIGN AND SYNTHESIS

To understand the influence of secondary structure on polymer dynamics, and vice versa, two sets of peptides were chosen (**Fig. 1**). Firstly, we studied polymers derived from a helical peptide. We employed as a guide, a crystal structure of a peptide (Boc-WIABIVBLBP-OMe)[40] which is α-helical due to the high content of 2-aminoisobutyric acid (Aib, B) residues. We then mutated the sequence to further promote helicity by specifically replacing the tryptophan and proline with lysine and alanine, and added additional glutamic acid residues for solubility, to generate the sequence KIABAVBLBAEE ("E-alpha"). Lysine, alanine, and glutamic acid are known to favor helical arrangements in proteins.[41,42] We also synthesized a sequence flipping the charged peptides to match the macrodipole of a helix (EIABAVBLBAKK, "K-alpha"), as it is established that positively charged residues at the negatively-charged C-terminal end promote greater helix stability.[43,44] A third peptide was synthesized by replacing alanine with the helix-directing amino acid Aib (EIAAAVALAAKK, "A-alpha"). Secondly, we designed a random coil peptide sequence with a high proportion of glycine and serine, with one arginine and one glutamic acid to promote water solubility (GSGSGRGSGSGE, "random"). This particular peptide is thus water soluble without being likely to fold into any defined secondary structure, and its lack of defined structure was further supported using AlphaFold2 (**Fig. 1e**).[45]

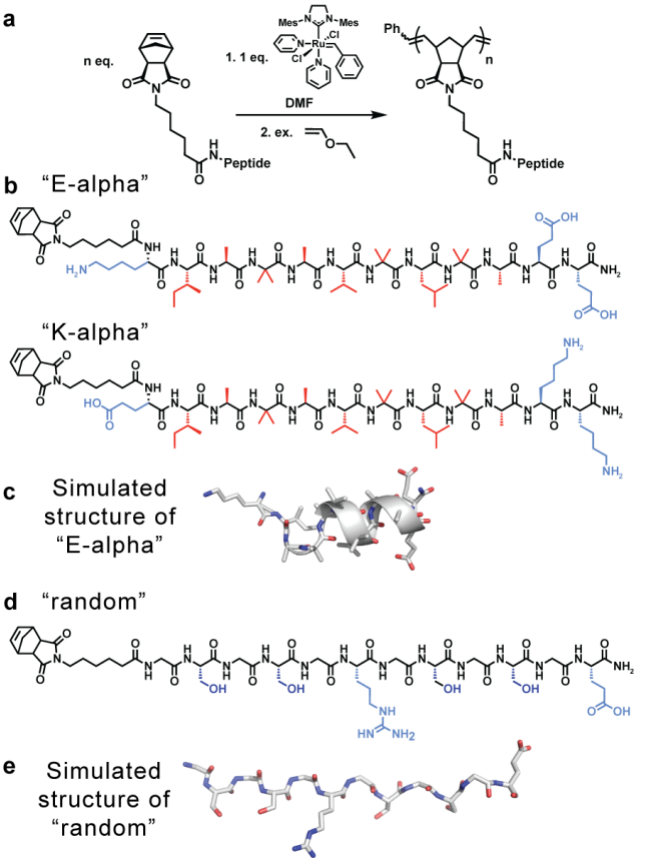

Figure 1. (**a**) Scheme showing the synthesis of peptide-brush polymers using graft-through ROMP. (**b**) Peptide sequences of α-helical monomers utilized to generate peptide-brush polymers, including E-alpha (sequence = NorAhaKIABAVBLBAEE) and K-alpha (sequence = NorAhaEIABAVBLBAKK), with hydrophobic residues indicated in red and hydrophilic residues indicated in blue. (**c**) Model of E-alpha peptide obtained from molecular dynamics simulations. (**d**) Peptide sequence of random coil peptide monomer utilized to generate peptide-brush polymers (sequence = NorAhaGSGSGRGSGSGE), with hydrophilic residues indicated in blue. (**e**) Model of random peptide obtained using AlphaFold2.[33]

The peptides were synthesized with *exo*-norbornene-2,3-dicarboxyimide attached via an aminohexanoic acid linker (denoted as "NorAha") at the N-terminus using established SPPS chemistry (SI Section 2 and SI **Fig. S1-S8**).[46] After purification, the resulting peptide macromonomers were polymerized via ROMP to degrees of polymerization (DPs) of 15, 30, and 45 (SI Section 3). Additional DPs of 7 and 90 were prepared for the helical sequence, E-alpha. All polymerizations were monitored by ^{1}H NMR spectroscopy (SI **Fig. S9-S11**). The molecular weights and polymer dispersities were determined by size exclusion chromatography coupled with multi-angle light scattering (SEC-MALS) and via sodium dodecyl sulfate–polyacrylamide gel electrophoresis (SDS-PAGE) (**Fig. 2**, **Table 1**, and SI **Fig. S12-14**). The resulting polymers were analyzed by dynamic light scattering revealing the polymers were not aggregated, with radii of hydration in aqueous solutions ranging

from 2 to 4 nanometers (**SI Table S1**). We note that the A-alpha sequence could not be polymerized due to intractable aggregation of the monomer during polymerization. However, this peptide served as a reference for CD spectroscopy (see SI **Fig. S15**).

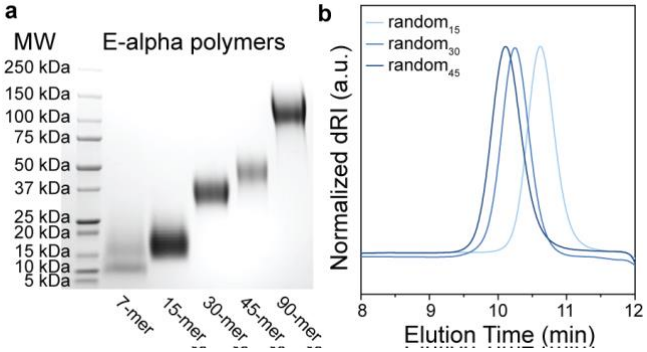

Figure 2. (**a**) SDS-PAGE gel of E-alpha polymers and the molecular weight ladder (MW), showing the approximate molecular weight distributions of each polymer. (**b**) Aqueous SEC-MALS of random peptide-based polymers (blue traces).

Table 1. Characterization of polymers, including theoretical molecular weight M_n, experimental M_w and M_n, dispersity ($Đ$), and approximate average molecular weight MW.

Polymer Sample	Theoretical M_n (kDa)	Experimental M_w / M_n (kDa)[a]	$Đ$ (M_w/M_n)[a]	MW (kDa)[b]
E-alpha$_7$	10	–	–	11
E-alpha$_{15}$	22	–	–	18
E-alpha$_{30}$	44	–	–	37
E-alpha$_{45}$	66	–	–	50
E-alpha$_{90}$	131	–	–	120
random$_{15}$	19	18.8 / 18.6	1.01	20
random$_{30}$	38	40.7 / 40.5	1.01	30
random$_{45}$	56	53.0 / 51.5	1.03	50
random$_{90}$	112.70	–	–	95

[a] M_w and M_n values for E-alpha PLPs could not be determined as SDS-PAGE, the only method by which the molecular weight of the polymer sample could be measured, does not allow for the determination of these values. Further details are provided in SI Section 2, and additional polymer characterization is listed in **SI Table S1**.

[b] MW values determined by estimating the middle of the sample band via visual inspection of SDS-PAGE data (**Fig. 2 and Figs. S11-S14**).

CHARACTERIZATION OF PEPTIDE BRUSH FOLDING BY CD SPECTROSCOPY

The secondary structures of free peptide monomers and polymers were determined by CD spectroscopy (**Fig. 3** and SI Section 4, see SI **Fig. S15-22**). Generally, the polymers displayed consistent structures to those of the monomeric peptides, with the glycine-serine repeat peptide and polymers showing characteristic features of random coil structure (**Fig. 3**). Likewise, the designed helical peptides displayed a strong maximum at 195 nm, and two minima at approximately 205 and 220 nm in 50% methanol and 100% methanol, indicative of helicity (**Fig. 3** and **SI Fig. S18** respectively).[47] The polymers of the two sequences match the CD spectra of the monomer when all are plotted relative to the concentration of the monomer unit. Additionally, the α-helical signal in 100% methanol (at 193 nm, 29 x10^3 deg•cm^2/dmol) is stronger than in 50% methanol (at 193 nm, 13-16 x10^3 deg•cm^2/dmol), indicating that the more hydrophobic solvent promotes the intramolecular hydrogen bonding of the peptide backbone amides necessary for the α-helical fold.

Intriguingly, in aqueous buffer, the polymers of E-alpha and K-alpha maintain a strong helical signal, while the peptide monomers are almost completely unfolded (10–16% helicity by analysis of CD data detailed in SI Section 4 and **SI Tables S2-3**). The intensity of helicity of the sample is clearly related to the degree of polymerization, with shorter polymers having less helical character (5% and 24% for E-alpha$_7$ and E-alpha$_{15}$ respectively), and longer polymers having greater degrees of helicity (43% and 46% for E-alpha$_{45}$ and E-alpha$_{90}$ respectively). This result suggests that the organization of peptide units along the polymer backbone generates a local hydrophobic environment, ascribed to the norbornene linker as well as the large proportion of hydrophobic side chains on E-alpha. This hydrophobic environment promotes the intramolecular hydrogen bonding of the peptide, much like that observed in methanol. However, the intensity of the signal in water is still lower than that observed in methanol, likely due to the dynamic nature of the polymer leading to globular, crowded conformations. This result is consistent with previous simulations and enzymatic assays,[18,20,21] where the polymer evades proteolysis of otherwise susceptible peptides.

The helical CD signal of the polymer is also relatively temperature stable. When the 30-mer is heated to 90 ºC, while some intensity at 220 nm is lost, the polymer's degree of secondary structure is completely regained when the sample is cooled back to room temperature (SI **Fig. S21**). These variable temperature curves do not show a clear sigmoidal melting transition (SI **Fig. S22**), similar to other variable temperature CD studies performed on helical peptides in water,[48,49] indicating that the folding of the polymer does not behave in a cooperative, two-state fashion. Additionally, despite the loss of some helicity at elevated temperatures, the polymer backbone allows the peptide to reversibly recover its folding patterns when cooled back to room temperature.

Well-tempered metadynamics simulations supported the probability of α-helix of around 10% for the E-alpha peptide-based macromonomer (**Fig. 4** and SI **Figs. S23-S25**). Further analyses showed that the central portion of the peptide strongly favors the formation of α-helix configuration (inset of **Fig. 4**, **Fig. S24**. These results correlate well with the experimental data, which supports 10% helical content in the peptide monomer by CD spectroscopy (**Table S2** and **Table S3**). Although metadynamics simulations of the secondary structure of the E-alpha$_{15}$ polymer did not converge despite considerable computational time (SI Section 5), hindering computational confirmation of the helicity observed, the consistency observed with monomer folding indicates that the polymer environment likely significantly alters the folding of the peptide sidechains.

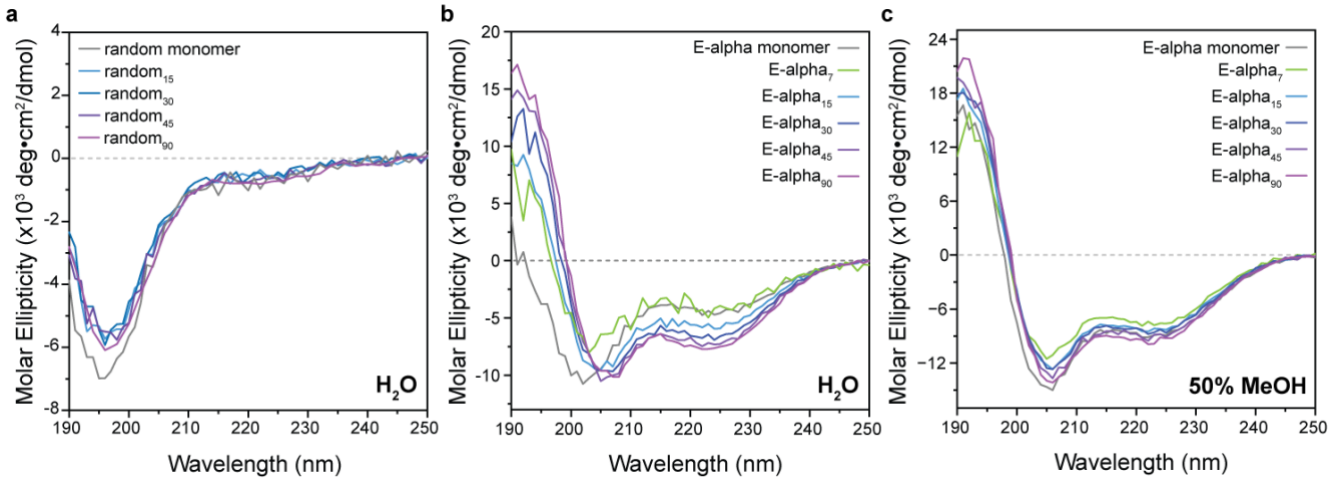

Figure 3. Circular dichroism (CD) spectra of (**a**) random coil peptide-based monomer and polymers in water and (**b**) α-helical peptide (E-alpha)-based monomer and polymers in 50 mM sodium carbonate buffer, and (**c**) helical peptide-based monomer and polymers in 50% methanol with 50 mM sodium carbonate buffer.

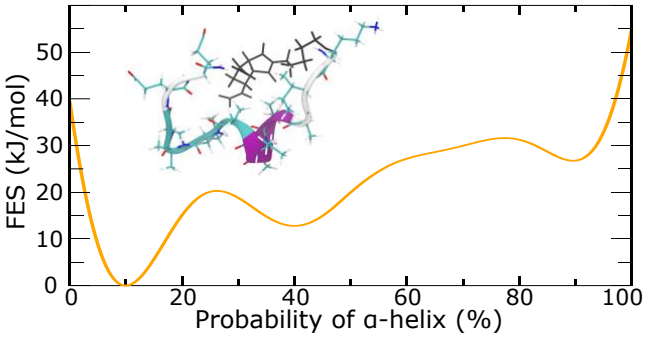

Figure 4. Free energy surface as a function of the probability of α-helix for E-alpha obtained from well-tempered metadynamics simulations. A probability of 10% is the most energetically stable with a characteristic structure provided in the inset. The α-helix/turn/random coil secondary structures of the peptide backbone are colored in magenta/cyan/white, respectively; NorAha atoms are colored in black.

NMR SPECTROSCOPY REVEALS FEATURES OF ALPHA HELICAL FOLDING BY PEPTIDE BRUSHES

In conjunction with CD spectroscopy, NMR spectroscopic studies of peptides and proteins provide critical insight into their structure. For example, the rate of exchange of amide protons with solvent protons is slowed down by intramolecular hydrogen bonding, such as that which results in folded peptide or protein structures.[50] As a result, a qualitative understanding of solvent-exposed regions of samples can be obtained by experiments where samples are dissolved in deuterium oxide, and the disappearance of peaks corresponding to exchangeable protons, like amide NH peaks, is monitored. Such experiments were conducted using D_2O and CD_3OD on the helical peptide-based monomer K-alpha and its resulting 15-mer polymer (**Fig. 5** and SI **Fig. S26-S43**).

We focused on these and subsequent NMR studies of the K-alpha monomer and K-alpha$_{15}$ polymer due to the basic conditions needed to dissolve the E-alpha peptide-based samples, which hinder analysis of the amide NH peaks due to their rapid exchange in basic solution.[51,52]

Samples were dissolved and then monitored by ^{1}H NMR spectroscopy over time, showing that in D_2O, samples generally show rapid disappearance of all NH peaks within one hour (**Fig. 5** and SI **Fig. S43**). In contrast, in CD_3OD both peptide monomer and polymer retain many amide signals, with the peptide monomer displaying less rapid amide peak disappearance in comparison to the polymer (**Fig. 5** and SI **Fig. S43**). Specifically, the polymer retains only three amide peaks after one hour, whereas the monomer retains eleven peaks. The retained polymer peaks correspond to the NH moieties of Aib7, Leu8, and Aib9, while in the monomer case, only the Glu1 NH peak disappears. The large difference between the monomer and polymer in methanol indicates that although peptides appear to be folded to the same degree by CD spectroscopy, the polymeric system appears to be more dynamic than the monomer in methanol, leading to an increased number of interactions with the solvent that result in a more rapid loss of signal. We note that more internal amino acids in the polymer case are retained (Aib7 to Aib9), with a gradual loss of intensity of residues next to this segment (Aib4, Ala5, and Val6). The amino acids that retain intensity correspond well to residues identified in metadynamics simulations of the E-alpha peptide monomer that are more likely to be helical, specifically, B4 to L8 (**Fig. 4-5**). In contrast, the NMR spectra of the peptide monomer only shows loss of the Glu1 NH peak, which is right next to the norbornene unit, and is consistent with observations that helices unfold by fraying at the peptide ends.[53,54] The amino acids at the ends of the helix are thus more likely to have interactions with solvent and thus show loss of intensity in the CD_3OD experiment. The dynamicity of the K-alpha$_{15}$ polymer is replicated in exchange studies performed on the random peptide and random$_{15}$ polymer (SI **Fig. S42**), where the polymer shows more rapid exchange than the peptide.

In addition, 2D TOCSY and NOESY NMR spectra were obtained for the K-alpha peptide monomer and K-alpha$_{15}$ polymer in H_2O/D_2O and CD_3OH to determine the degree of folding of the two samples as a function of the solvent environment, as such experiments allow for the identification of secondary structure (SI **Fig. S32-41**). Qualitatively, we observe a much greater number of nuclear Overhauser effect (NOE) features in the samples dissolved in CD_3OH (e.g peptide 2D NOESY spectra in SI **Fig. S33-34** and **S36-37**; polymer 2D NOESY spectra in SI Fig. **S39-41**). Moreover, the polymer

spectra display a significant broadening of peaks in both H_2O/D_2O and CD_3OH relative to the peptide monomers (SI **Fig. S26-31**). This broadening is due to both the polymer dispersity and significant differences in the chemical environment along the polymer, as well as more efficient relaxation of the larger molecule (18 kDa vs. 1.5 kDa).

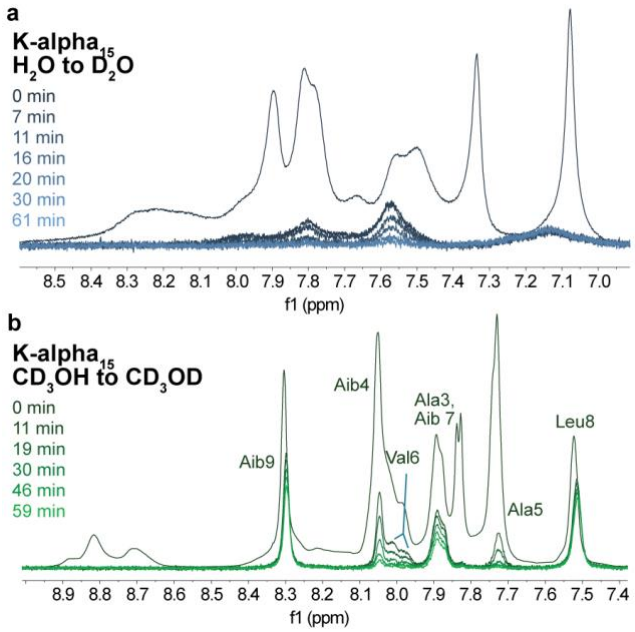

Figure 5. ^{1}H NMR spectra of the K-alpha$_{15}$ polymer. (**a**) Dissolved in 100% D_2O (blue traces). (**b**) Dissolved in 100% CD_3OD (green traces). Analysis shows the disappearance of NH amide peaks of the peptide brush sequence upon exchange with the deuterated solvent. The spectra at 0 min were obtained from separate experiments where samples were dissolved in 90% H_2O with 10% D_2O or 100% CD_3OH. The sample dissolved in CD_3OD shows a slower loss of peaks, likely due to the greater folding observed in this solvent.

The K-alpha peptide monomer displays some slight evidence of helicity in H_2O/D_2O, and even more clear evidence of helicity in CD_3OH, with strong NOE signals of NN(*i*, *i*+1) NOEs in both being visible, as well as (*i*, *i*+4) NOEs in CD_3OH (SI **Fig. S36-37**). We also note that the J-coupling values and Hα positions of most amino acids, though likely perturbed due to being in CD_3OH, are more consistent with α-helicity than random coil values.[55–57]

While the broadness of the polymer data in H_2O/D_2O hinders further analysis, the 2D NMR data of the sample dissolved in CD_3OH allows for the identification of the positions of NH and Hα peaks corresponding to each amino acid of the monomer unit (SI **Fig. S31**). Of interest is that the positions of Glu1, Ile2, and Ala3 shift significantly downfield relative to their position in the peptide monomer spectra, suggesting that these NH groups experience a substantial change in their chemical environment that is consistent with their position proximal to the norbornene-based linker and polymer backbone. Interestingly, Glu1, Ile2, and Val6 broaden significantly and display two distinct peaks, possibly indicative of an intermediate chemical exchange between two conformations of peptide folding. While significant overlap of the peaks of some residues (*i.e.* Ha of Ala3 and Ala5) hinders further analysis, NOEs between the Ha of Val6 and NH peaks of *i*+1 (Aib7), *i*+2 (Leu8), *i*+3 (Aib9), and *i*+4 (Ala10) residues can be identified, establishing the helical character of this segment in the polymer (SI **Fig. S41**).

POLYMER CONFORMATION: INSIGHT FROM SAXS AND CRYO-TEM DATA

In addition to the information obtained by CD spectroscopy, we sought to obtain greater structural insight using small-angle X-ray scattering (SAXS). Solutions of polymers dissolved in a range of solvents were prepared and analyzed (**Fig. 6**; SI Section 7 **Tables S4–S11** and **Figs. S44-S57**). In all cases, the peptide-brush polymers displayed approximately globular conformations, with a clear maximum near the ideal values for a compact sphere in the normalized Kratky plot, which is a peak in $(qR_g)2I_{(q)}/I_{(0)}$ of 1.104 at $qR_g \sim 1.73$ (**Fig. 6**). Consistent with studies of other types of brush polymers that longer polymers are more rod-like, as opposed to star-like at shorter lengths, the 90-mer polymers of the helical peptide and random coil peptide monomers have a normalized Kratky plot with a maximum at greater values than that of the ideal sphere (magenta traces in **Fig. 6a, c,** and **d**).[58]

In contrast to the results of PLPs dissolved in aqueous solutions, the E-alpha peptide brush polymers in 50% and 100% methanol solutions show much greater extension and flexibility (**Fig. 6d** and SI **Fig. S47-49**). Guinier analysis generally yields R_g values much larger than those for the same samples measured in aqueous buffers, and Guinier-Porod analysis yields larger values of *s*, indicative of greater rod-like character (SI **Table S4** and **S7**).[59] Additionally, the normalized Kratky plots of these samples in methanol deviate significantly from an ideal bell curve representative of a compact sphere or globule. These results are consistent with the observation that the more hydrophobic solvent mixtures are better able to solvate the hydrophobic polymer backbone. The greater helicity observed in these polymers by CD and NMR spectroscopy is supported by the more extended polymer conformations observed via SAXS, wherein more rigid helical side chains resist collapse of the polymers into more globular structures. This deviation from globularity in 50% methanol of the helical PLPs can be contrasted to the SAXS data and normalized Kratky plots of scattering from the random coil PLPs, which show little change relative to the Kratky plots of the polymers in water (**Fig. 6a** and **b**). This result suggests that degree of solvation of the hydrophobic polymer backbone is not the key factor influencing conformation here, but rather the peptide plays a significant role. Importantly, this suggests that peptide structure can be designed to influence polymer conformations and their prevalence in particular environments.

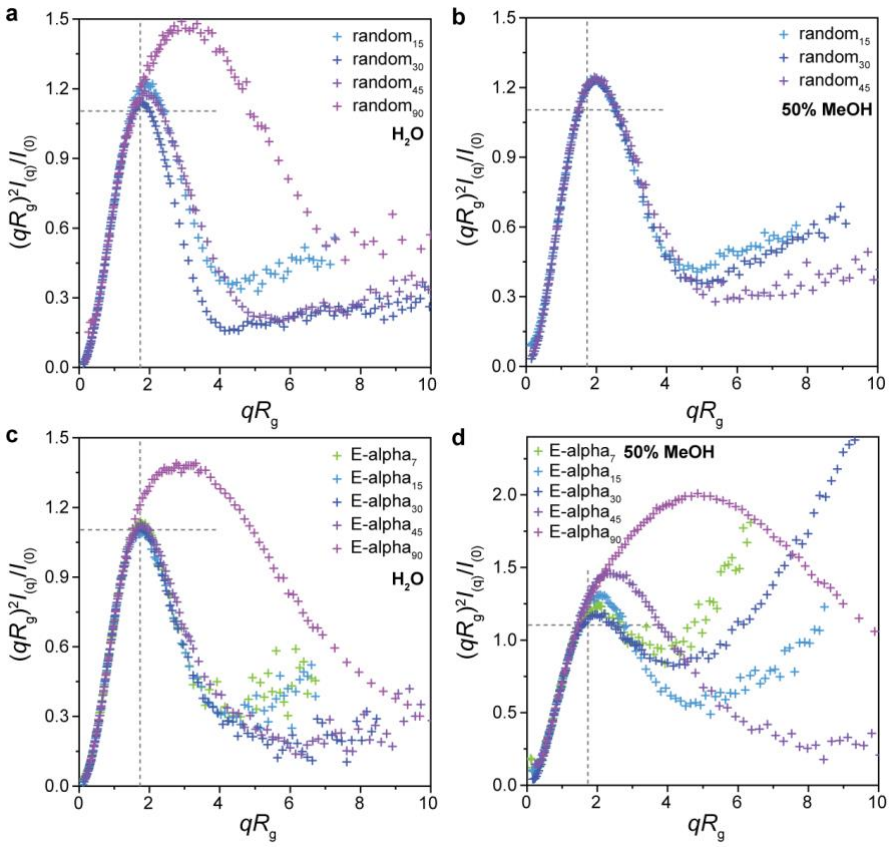

Figure 6. Normalized Kratky plots of SAXS data of random (**a, b**) and α-helical brush-polymers derived from the E-alpha peptide sequence (**c, d**) in water and 50% methanol. The dashed lines indicate the values for an ideal compact sphere (qR_g = 1.73 and $(qR_g)2I_{(q)}/I_{(0)}$ = 1.1).

Atomistic metadynamics simulations, while unable to equilibrate sufficiently, did provide structural models of the E-alpha$_{15}$ polymer that were consistent with CD spectroscopy data in that a portion of the peptide sidechains was folding as α-helices (**Fig. 4**). We wished to corroborate whether the models were consistent with the SAXS data provided. Accordingly, we fit the experimental SAXS pattern of E-alpha$_{15}$ in aqueous buffer to one such model using the FoXS server,[60,61] resulting in a goodness-of-fit parameter of χ^2 = 0.47 (**Fig. 8**). This correspondence between the *in silico* model and the experimental data indicates that the model may be a reasonable representation of the polymer's conformation at longer length-scales (>1 nm), and lends further insight into the structure of these polymers complementary to the structural data obtained from spectroscopic studies.

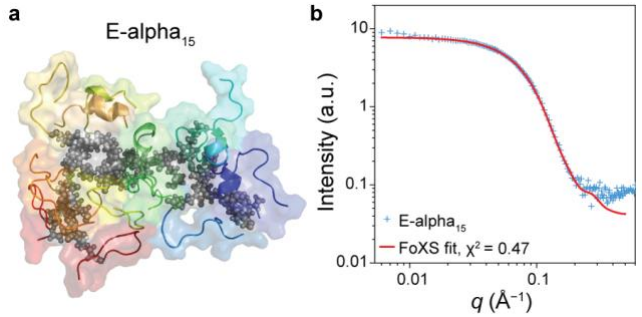

Figure 7. (**a**) Atomistic simulation structure of E-alpha$_{15}$. (**b**) Fit of E-alpha$_{15}$ structure from simulations to the experimental SAXS pattern of E-alpha$_{15}$.

To provide additional insight into polymer conformation in solution, cryogenic transmission electron microscopy (cryo-TEM) was employed (SI Section 8). This technique has been successfully utilized to visualize conjugated polymers,[62] self-assembling amphiphilic polymers,[63,64] and dendritic polymers.[65] The size of lower molecular weight polymers in this work, of up to approximately 45 kDa, suggested that these samples might be challenging to observe via cryo-TEM.[66,67] However, we anticipated that alpha$_{90}$, which has an approximate molecular weight of 120 kDa could provide enough contrast. Indeed, the resulting micrographs of aqueous, unstained E-alpha$_{90}$ revealed distinct, low-dispersity particles aligning closely with the size range predicted by the SAXS data, averaging around 16 ± 1 nm in diameter (**Fig. 8**). Particle shapes appear roughly spherical, which is likewise consistent with the observed sizes, which are more collapsed than would be anticipated based on the polymer length, as well as the SAXS data that suggests a collapsed polymer conformation. We note that these micrographs are similar to cryo-TEM results obtained for single-chain nanoparticles[37] and PEGylated bottlebrush polymers.[68]

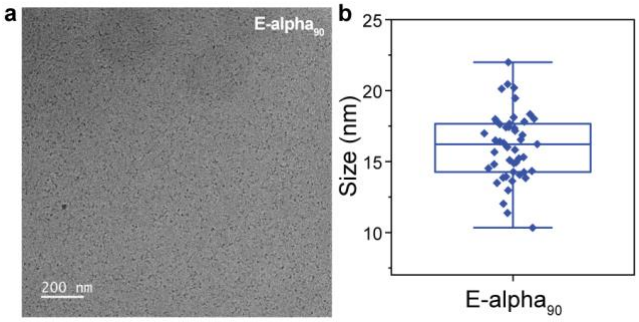

Figure 8. (**a**) Cryo-TEM micrograph of unstained E-alpha$_{90}$ frozen in aqueous sodium carbonate buffer. (**b**) Size distribution analysis of particles found in the micrograph. Average particle size is 16 ± 1 nm. The image was acquired with a total accumulated dose of 16.49 $e^{-}/Å^2$.

CONCLUSIONS

In conclusion, we describe a structural interrogation of peptide-brush polymers incorporating α-helical peptide-based monomers, as well as a random coil-based peptide monomer. These peptides and polymers were investigated using CD spectroscopy, NMR spectroscopy, small-angle X-ray scattering, and atomistic metadynamics simulations, confirming key differences in peptide folding on the polymer backbone, as well as the overall polymer conformation. Specifically, the polymer environment appears to enforce a greater degree of helicity than is present in peptide monomers, which increases in magnitude as the degree of polymerization increases. NMR studies confirm the helicity for the polymer structures and that helical folding is concentrated in central residues of the peptide sequence in both monomer and polymer brushes. SAXS analysis confirms that while both sets of polymers are compact and globular in aqueous environments, the α-helical peptide-brush polymers are more extended and flexible in more hydrophobic solvents, consistent with the greater helicity observed in these environments. This result suggests that peptide brushes that are completely folded may resist forming compact polymeric structures, which would make the peptides more accessible to protein targets of interest as well as proteolytic enzymes. Overall, this demonstration of the tunability of polymer conformation and peptide brush folding is a key insight guiding future designs as we seek to mimic both functional and structural aspects of proteins and to engage natural proteins in specific ways for the development of peptide brush polymers as proteomimetic therapeutics and functional materials.

ASSOCIATED CONTENT

Supporting Information

The Supporting Information is available free of charge on the ACS Publications website.

General considerations; synthesis and characterization of peptides and polymers; methods of spectroscopy, scattering, and simulations (PDF)

AUTHOR INFORMATION

Corresponding Author

* nathan.gianneschi@northwestern.edu

Author Contributions

All authors have given approval to the final version of the manuscript.

Funding Sources

NSF DMR-2004899

ACKNOWLEDGMENT

This work was supported by the National Science Foundation (NSF) under award number DMR-2004899. J.O. acknowledges support through an NIH NRSA F32 fellowship from the National Institute of General Medical Sciences (NIGMS; F32GM143925). O.E. acknowledges support from the NSF Graduate Research Fellowship (Grant No. 2234667). N.R. acknowledges support from the Ryan Fellowship and the International Institute for Nanotechnology at Northwestern University (NU).
This work made use of the IMSERC MS and NMR facility at NU, which has received support from the Soft and Hybrid Nanotechnology Experimental (SHyNE) Resource (NSF ECCS-2025633), and NU; the NMR facility has also support from NIH 1S10OD012016-01 / 1S10RR019071-01A1. Work was performed at the BioCryo and Keck-II facilities of NU's NUANCE Center, which have received support from the SHyNE Resource (NSF ECCS-2025633), the IIN, and Northwestern's MRSEC program (NSF DMR-2308691). Additionally, this work used instruments in the Keck Biophysics Facility, a shared resource of the Robert H. Lurie Comprehensive Cancer Center of NU supported in part by the NCI Cancer Center Support Grant P30 CA060553. SAXS data was measured at Beamline 16ID (LiX) of the National Synchrotron Light Source II, part of the Center for BioMolecular Structure (CBMS), which is supported by the NIH NIGMS (P30GM133893) and by the Department of Energy (DOE) Office of Biological and Environmental Research (KP1605010). LiX also received additional support from NIH Grant S10 OD012331. Work performed at the CBMS is supported in part by the U.S. DOE Office of Science, Office of Basic Energy Sciences Program under contract number DE-SC0012704. Additional SAXS data was collected at the DuPont-Northwestern-Dow Collaborative Access Team (DND-CAT) located at Sector 5 of the Advanced Photon Source (APS). DND-CAT is supported by NU, The Dow Chemical Company, and DuPont de Nemours, Inc. The APS is a U.S. DOE Office of Science User Facility operated for the DOE Office of Science by Argonne National Laboratory under Contract No. DE-AC02-06CH11357. Data at DND-CAT was collected using an instrument funded by the NSF (Award Number 0960140). K.S. and B.Q. acknowledge the Texas Advanced Computing Center (TACC) at the University of Texas at Austin for the computational resources used in this work. This work benefited from the use of the SasView application, originally developed under NSF award DMR-0520547. SasView contains code developed with funding from the European Union's Horizon 2020 research and innovation program under the SINE2020 project, grant agreement No 654000. Images of peptides and polymers in Figs. 1 and 7 were prepared using PyMol v. 2.5.0. We thank Dr. Lin Yang, Dr. Or Berger, Dr. Nicholas Hampu, Prof. Hao Sun, Prof. Andy Nguyen, Navjit Paul, Madeline Hopps, Mara Fattah, and Dr. Yongbo Zhang for helpful discussions and experimental assistance in the course of this study.

REFERENCES

(1) Bray, B. L. Large-Scale Manufacture of Peptide Therapeutics by Chemical Synthesis. *Nat. Rev. Drug Discov.* **2003**, *2* (7), 587–593.

(2) Vagner, J.; Qu, H.; Hruby, V. J. Peptidomimetics, a Synthetic Tool of Drug Discovery. *Curr. Opin. Chem. Biol.* **2008**, *12* (3), 292–296.

(3) Fosgerau, K.; Hoffmann, T. Peptide Therapeutics: Current Status and Future Directions. *Drug Discov. Today* **2015**, *20* (1), 122–128.

(4) Muttenthaler, M.; King, G. F.; Adams, D. J.; Alewood, P. F. Trends in Peptide Drug Discovery. *Nat. Rev. Drug Discov.* **2021**, *20* (4), 309–325.

(5) Al Musaimi, O.; Lombardi, L.; Williams, D. R.; Albericio, F. Strategies for Improving Peptide Stability and Delivery. *Pharmaceuticals* **2022**, *15* (10), 1283.

(6) Malins, L. R.; Degruyter, J. N.; Robbins, K. J.; Scola, P. M.; Eastgate, M. D.; Ghadiri, M. R.; Baran, P. S. Peptide Macrocyclization Inspired by Non-Ribosomal Imine Natural Products. *J. Am. Chem. Soc.* **2017**, *139* (14), 5233–5241.

(7) Kessler, H. Conformation and Biological Activity of Cyclic Peptides. *Angew. Chemie Int. Ed. English* **1982**, *21* (7), 512–523.

(8) Kohli, R. M.; Walsh, C. T.; Burkart, M. D. Biomimetic Synthesis and Optimization of Cyclic Peptide Antibiotics. *Nature* **2002**, *418* (6898), 658–661.

(9) Lau, J.; Bloch, P.; Schäffer, L.; Pettersson, I.; Spetzler, J.; Kofoed, J.; Madsen, K.; Knudsen, L. B.; McGuire, J.; Steensgaard, D. B.; Strauss, H. M.; Gram, D. X.; Knudsen, S. M.; Nielsen, F. S.; Thygesen, P.; Reedtz-Runge, S.; Kruse, T. Discovery of the Once-Weekly Glucagon-Like Peptide-1 (GLP-1) Analogue Semaglutide. *J. Med. Chem.* **2015**, *58* (18), 7370–7380.

(10) Berndt, P.; Fields, G. B.; Tirrell, M. Synthetic Lipidation of Peptides and Amino Acids: Monolayer Structure and Properties. *J. Am. Chem. Soc.* **1995**, *117* (37), 9515–9522.

(11) Chen, B.; Sun, Y.; Niu, J.; Jarugumilli, G. K.; Wu, X. Protein Lipidation in Cell Signaling and Diseases: Function, Regulation, and Therapeutic Opportunities. *Cell Chem. Biol.* **2018**, *25* (7), 817–831.

(12) Kim, Y.-W.; Grossmann, T. N.; Verdine, G. L. Synthesis of All-Hydrocarbon Stapled α-Helical Peptides by Ring-Closing Olefin Metathesis. *Nat. Protoc.* **2011**, *6* (6), 761–771.

(13) Castro, C. E.; Kilchherr, F.; Kim, D.; Shiao, E. L.; Wauer, T.; Wortmann, P.; Bathe, M.; Dietz, H. A Primer to Scaffolded DNA Origami. **2011**, *8* (3), 221–229.

(14) Spokoyny, A. M.; Zou, Y.; Ling, J. J.; Yu, H.; Lin, Y.; Pentelute, B. L. A Perfluoroaryl-Cysteine S N Ar Chemistry Approach to Unprotected Peptide Stapling. *J. Am. Chem. Soc.* **2013**, *135* (16), 5946–5949.

(15) Horne, W. S.; Grossmann, T. N. Proteomimetics as Protein-Inspired Scaffolds with Defined Tertiary Folding Patterns. *Nat. Chem.* **2020**, *12* (4), 331–337.

(16) Horne, W. S. Peptide and Peptoid Foldamers in Medicinal Chemistry. *Expert Opin. Drug Discov.* **2011**, *6* (12), 1247–1262.

(17) Kammeyer, J. K.; Blum, A. P.; Adamiak, L.; Hahn, M. E.; Gianneschi, N. C. Polymerization of Protecting-Group-Free Peptides via ROMP. *Polym. Chem.* **2013**, *4* (14), 3929–3933.

(18) Blum, A. P.; Kammeyer, J. K.; Yin, J.; Crystal, D. T.; Rush, A. M.; Gilson, M. K.; Gianneschi, N. C. Peptides Displayed as High Density Brush Polymers Resist Proteolysis and Retain Bioactivity. *J. Am. Chem. Soc.* **2014**, *136* (43), 15422–15437.

(19) Sun, H.; Choi, W.; Zang, N.; Battistella, C.; Thompson, M. P.; Cao, W.; Zhou, X.; Forman, C.; Gianneschi, N. C. Bioactive Peptide Brush Polymers via Photoinduced Reversible-Deactivation Radical Polymerization. *Angew. Chem. Int. Ed.* **2019**, *58* (48), 17359–17364.

(20) Sun, H.; Qiao, B.; Choi, W.; Hampu, N.; McCallum, N. C.; Thompson, M. P.; Oktawiec, J.; Weigand, S.; Ebrahim, O. M.; de la Cruz, M. O.; Gianneschi, N. C. Origin of Proteolytic Stability of Peptide-Brush Polymers as Globular Proteomimetics. *ACS Cent. Sci.* **2021**, *7* (12), 2063–2072.

(21) Blum, A. P.; Kammeyer, J. K.; Gianneschi, N. C. Activating Peptides for Cellular Uptake via Polymerization into High Density Brushes. *Chem. Sci.* **2016**, *7* (2), 989–994.

(22) Blum, A. P.; Nelles, D. A.; Hidalgo, F. J.; Touve, M. A.; Sim, D. S.; Madrigal, A. A.; Yeo, G. W.; Gianneschi, N. C. Peptide Brush Polymers for Efficient Delivery of a Gene Editing Protein to Stem Cells. *Angew. Chemie* **2019**, *131* (44), 15793–15796.

(23) Choi, W.; Nensel, A. K.; Droho, S.; Fattah, M. A.; Mokashi-Punekar, S.; Swygart, D. I.; Burton, S. T.; Schwartz, G. W.; Lavine, J. A.; Gianneschi, N. C. Thrombospondin-1 Proteomimetic Polymers Exhibit Anti-Angiogenic Activity in a Neovascular Age-Related Macular Degeneration Mouse Model. *Sci. Adv.* **2023**, *9* (41), eadi8534.

(24) Carrow, K. P.; Hamilton, H. L.; Hopps, M. P.; Li, Y.; Qiao, B.; Payne, N. C.; Thompson, M. P.; Zhang, X.; Magassa, A.; Fattah, M.; Agarwal, S.; Vincent, M. P.; Buyanova, M.; Bertin, P. A.; Mazitschek, R.; Olvera de la Cruz, M.; Johnson, D. A.; Johnson, J. A.; Gianneschi, N. C. Inhibiting the Keap1/Nrf2 Protein-Protein Interaction with Protein-Like Polymers. *Adv. Mater.* **2024**, 1–36.

(25) Callmann, C. E.; Thompson, M. P.; Gianneschi, N. C. Poly(Peptide): Synthesis, Structure, and Function of Peptide–Polymer Amphiphiles and Protein-like Polymers. *Acc. Chem. Res.* **2020**, *53* (2), 400–413.

(26) Wang, J.; Lu, H.; Ren, Y.; Zhang, Y.; Morton, M.; Cheng, J.; Lin, Y. Interrupted Helical Structure of Grafted Polypeptides in Brush-like Macromolecules. *Macromolecules* **2011**, *44* (22), 8699–8708.

(27) Baumgartner, R.; Fu, H.; Song, Z.; Lin, Y.; Cheng, J. Cooperative Polymerization of α-Helices Induced by Macromolecular Architecture. *Nat. Chem.* **2017**, *9* (7), 614–622.

(28) Marullo, R.; Kastantin, M.; Drews, L. B.; Tirrell, M. Peptide Contour Length Determines Equilibrium Secondary Structure in Protein-Analogous Micelles. *Biopolymers* **2013**, *99* (9), 573–581.

(29) Yu, Y. C.; Tirrell, M.; Fields, G. B. Minimal Lipidation Stabilizes Protein-like Molecular Architecture. *J. Am. Chem. Soc.* **1998**, *120* (39), 9979–9987.

(30) Kastantin, M.; Tirrell, M. Helix Formation in the Polymer Brush. *Macromolecules* **2011**, *44* (12), 4977–4987.

(31) Pelay-Gimeno, M.; Glas, A.; Koch, O.; Grossmann, T. N. Structure-Based Design of Inhibitors of Protein-Protein Interactions: Mimicking Peptide Binding Epitopes. *Angew. Chemie - Int. Ed.* **2015**, *54* (31), 8896–8927.

(32) Rezaei Araghi, R.; Keating, A. E. Designing Helical Peptide Inhibitors of Protein-Protein Interactions. *Curr. Opin. Struct. Biol.* **2016**, *39*, 27–38.

(33) Upadhya, R.; Murthy, N. S.; Hoop, C. L.; Kosuri, S.; Nanda, V.; Kohn, J.; Baum, J.; Gormley, A. J. PET-RAFT and SAXS: High Throughput Tools to Study Compactness and Flexibility of Single-Chain Polymer Nanoparticles. *Macromolecules* **2019**, *52* (21), 8295–8304.

(34) Berda, E. B.; Foster, E. J.; Meijer, E. W. Toward Controlling Folding in Synthetic Polymers: Fabricating and Characterizing Supramolecular Single-Chain Nanoparticles. *Macromolecules* **2010**, *43* (3), 1430–1437.

(35) Murnen, H. K.; Khokhlov, A. R.; Khalatur, P. G.; Segalman, R. A.; Zuckermann, R. N. Impact of Hydrophobic Sequence Patterning on the Coil-to-Globule Transition of Protein-like Polymers. *Macromolecules* **2012**, *45* (12), 5229–5236.

(36) Ter Huurne, G. M.; Gillissen, M. A. J.; Palmans, A. R. A.; Voets, I. K.; Meijer, E. W. The Coil-to-Globule Transition of Single-Chain Polymeric Nanoparticles with a Chiral Internal Secondary Structure. *Macromolecules* **2015**, *48* (12), 3949–3956.

(37) Terashima, T.; Mes, T.; De Greef, T. F. A.; Gillissen, M. A. J.; Besenius, P.; Palmans, A. R. A.; Meijer, E. W. Single-Chain Folding of Polymers for Catalytic Systems in Water. *J. Am. Chem. Soc.* **2011**, *133* (13), 4742–4745.

(38) Barbee, M. H.; Wright, Z. M.; Allen, B. P.; Taylor, H. F.; Patteson, E. F.; Knight, A. S. Protein-Mimetic Self-Assembly with Synthetic Macromolecules. *Macromolecules* **2021**, *54* (8), 3585–3612.

(39) Lyon, C. K.; Prasher, A.; Hanlon, A. M.; Tuten, B. T.; Tooley, C. A.; Frank, P. G.; Berda, E. B. A Brief User's Guide to Single-Chain Nanoparticles. *Polym. Chem.* **2015**, *6* (2), 181–197.

(40) Karle, I. L.; Sukumar, M.; Balaram, P. Parallel Packing of α-Helices in Crystals of the Zervamicin IIA Analog Boc-Trp-Ile-Ala-Aib-Ile-Val-Aib-Leu-Aib-Pro-OMe·2H2O. *Proc. Natl. Acad. Sci. U. S. A.* **1986**, *83* (24), 9284–9288.

(41) Chou, P. Y.; Fasman, G. D. Prediction of Protein Conformation. *Biochemistry* **1974**, *13* (2), 222–245.

(42) Monera, O. D.; Sereda, T. J.; Zhou, N. E.; Kay, C. M.; Hodges, R. S. Relationship of Sidechain Hydrophobicity and A-helical Propensity on the Stability of the Single-stranded Amphipathic A-helix. *J. Pept. Sci.* **1995**, *1* (5), 319–329.

(43) Scholtz, M.; Robbins, V. H.; Baldwin, R. L. The Energetics of Ion-Pair and Hydrogen-Bonding Interactions In. **1993**, 9668–9676.

(44) Armstrong, K. M.; Baldwin, R. L. Charged Histidine Affects α-Helix Stability at All Positions in the Helix by Interacting with

the Backbone Charges. *Proc. Natl. Acad. Sci. U. S. A.* **1993**, *90* (23), 11337–11340.

(45) Mirdita, M.; Schütze, K.; Moriwaki, Y.; Heo, L.; Ovchinnikov, S.; Steinegger, M. ColabFold: Making Protein Folding Accessible to All. *Nat. Methods* **2022**, *19* (6), 679–682.

(46) Maynard, H. D.; Okada, S. Y.; Grubbs, R. H. Inhibition of Cell Adhesion to Fibronectin by Oligopeptide-Substituted Polynorbornenes. *J. Am. Chem. Soc.* **2001**, *123* (7), 1275–1279.

(47) Greenfield, N. J. Using Circular Dichroism Spectra to Estimate Protein Secondary Structure. *Nat. Protoc.* **2007**, *1* (6), 2876–2890.

(48) Greenfield, N. J. Using Circular Dichroism Collected as a Function of Temperature to Determine the Thermodynamics of Protein Unfolding and Binding Interactions. *Nat. Protoc.* **2007**, *1* (6), 2527–2535.

(49) Scholtz, J. M.; Marqusee, S.; Baldwin, R. L.; York, E. J.; Stewart, J. M.; Santoro, M.; Bolen, D. W. Calorimetric Determination of the Enthalpy Change for the α-Helix to Coil Transition of an Alanine Peptide in Water. *Proc. Natl. Acad. Sci. U. S. A.* **1991**, *88* (7), 2854–2858.

(50) Dempsey, C. E. Hydrogen Exchange in Peptides and Proteins Using NMR Spectroscopy. *Prog. Nucl. Magn. Reson. Spectrosc.* **2001**, *39* (2), 135–170.

(51) Wüthrich, K.; Wagner, G. Nuclear Magnetic Resonance of Labile Protons in the Basic Pancreatic Trypsin Inhibitor. *J. Mol. Biol.* **1979**, *130* (1), 1–18.

(52) Kurt Wüthrich - NMR of Proteins and Nucleic Acids (Baker Lecture Series)-Wiley-Interscience (1986).Pdf.

(53) Silva, R. A. G. D.; Kubelka, J.; Bour, P.; Decatur, S. M.; Keiderling, T. A. Site-Specific Conformational Determination in Thermal Unfolding Studies of Helical Peptides Using Vibrational Circular Dichroism with Isotopic Substitution. *Proc. Natl. Acad. Sci. U. S. A.* **2000**, *97* (15), 8318–8323.

(54) Diana, D.; Ziaco, B.; Scarabelli, G.; Pedone, C.; Colombo, G.; D'Andrea, L. D.; Fattorusso, R. Structural Analysis of a Helical Peptide Unfolding Pathway. *Chem. - A Eur. J.* **2010**, *16* (18), 5400–5407.

(55) Schwarzinger, S.; Kroon, G. J. A.; Foss, T. R.; Chung, J.; Wright, P. E.; Dyson, H. J. Sequence-Dependent Correction of Random Coil NMR Chemical Shifts. *J. Am. Chem. Soc.* **2001**, *123* (13), 2970–2978.

(56) Mielke, S. P.; Krishnan, V. V. Characterization of Protein Secondary Structure from NMR Chemical Shifts. *Prog. Nucl. Magn. Reson. Spectrosc.* **2009**, *54* (3–4), 141–165.

(57) Wishart, D. S.; Sykes, B. D.; Richards, F. M. Relationship between Nuclear Magnetic Resonance Chemical Shift and Protein Secondary Structure. *J. Mol. Biol.* **1991**, *222* (2), 311–333.

(58) Pesek, S. L.; Li, X.; Hammouda, B.; Hong, K.; Verduzco, R. Small-Angle Neutron Scattering Analysis of Bottlebrush Polymers Prepared via Grafting-through Polymerization. *Macromolecules* **2013**, *46* (17), 6998–7005.

(59) Wei, Y.; Hore, M. J. A. Characterizing Polymer Structure with Small-Angle Neutron Scattering: A Tutorial. *J. Appl. Phys.* **2021**, *129* (17).

(60) Schneidman-Duhovny, D.; Hammel, M.; Sali, A. FoXS: A Web Server for Rapid Computation and Fitting of SAXS Profiles. *Nucleic Acids Res.* **2010**, *38* (SUPPL. 2), 540–544.

(61) Schneidman-Duhovny, D.; Hammel, M.; Tainer, J. A.; Sali, A. Accurate SAXS Profile Computation and Its Assessment by Contrast Variation Experiments. *Biophys. J.* **2013**, *105* (4), 962–974.

(62) Zhou, Y. Y.; Xu, Y. C.; Yao, Z. F.; Li, J. Y.; Pan, C. K.; Lu, Y.; Yang, C. Y.; Ding, L.; Xiao, B. F.; Wang, X. Y.; Shao, Y.; Zhang, W. Bin; Wang, J. Y.; Wang, H.; Pei, J. Visualizing the Multi-Level Assembly Structures of Conjugated Molecular Systems with Chain-Length Dependent Behavior. *Nat. Commun.* **2023**, *14* (1).

(63) Smeltzer, S. E.; Sanders, C. A.; Liu, Y.; George, S. R.; Amiri, C.; Gernandt, A.; Reck, B.; Cunningham, M. F. Amphiphilic Block-Random Copolymers: Shedding Light on Aqueous Self-Assembly Behavior. *Macromolecules* **2023**, *56* (4), 1601–1614.

(64) Lee, J. Y.; Song, Y.; Wessels, M. G.; Jayaraman, A.; Wooley, K. L.; Pochan, D. J. Hierarchical Self-Assembly of Poly(d -Glucose Carbonate) Amphiphilic Block Copolymers in Mixed Solvents. *Macromolecules* **2020**, *53* (19), 8581–8591.

(65) Bae, Y.; Ha, M. Y.; Bang, K. T.; Yang, S.; Kang, S. Y.; Kim, J.; Sung, J.; Kang, S.; Kang, D.; Lee, W. B.; Choi, T. L.; Park, J. Conformation Dynamics of Single Polymer Strands in Solution. *Adv. Mater.* **2022**, *34* (32), 1–8.

(66) Herzik, M. A.; Wu, M.; Lander, G. C. High-Resolution Structure Determination of Sub-100 KDa Complexes Using Conventional Cryo-EM. *Nat. Commun.* **2019**, *10* (1), 1–9.

(67) Zhang, Y.; Tammaro, R.; Peters, P. J.; Ravelli, R. B. G. Could Egg White Lysozyme Be Solved by Single Particle Cryo-EM? *J. Chem. Inf. Model.* **2020**, *60* (5), 2605–2613.

(68) Detappe, A.; Nguyen, H. V. T.; Jiang, Y.; Agius, M. P.; Wang, W.; Mathieu, C.; Su, N. K.; Kristufek, S. L.; Lundberg, D. J.; Bhagchandani, S.; Ghobrial, I. M.; Ghoroghchian, P. P.; Johnson, J. A. Molecular Bottlebrush Prodrugs as Mono- and Triplex Combination Therapies for Multiple Myeloma. *Nat. Nanotechnol.* **2023**, *18* (2), 184–192.